JOURNAL OF SPACECRAFT AND ROCKETS
Vol. 32, No. 4, July–August 1995

Baffle Effect on Sloshing-Modulated Torques Responsed to Orbital Accelerations in Microgravity

R. J. Hung* and H. L. Pan†
University of Alabama in Huntsville, Huntsville, Alabama 35899

The behavior of sloshing-dynamics-modulated fluid systems driven by orbital accelerations including gravity gradient and jitter accelerations has been studied. Partly liquid-filled rotating Dewars applicable to a full-scale Gravity Probe-B Spacecraft container with and without baffle are considered. Results show that a slosh wave excited along the liquid-vapor interface induced by jitter-acceleration-dominated orbital accelerations provides a torsional moment with an up-and-down movement of bubble oscillations in the rotating Dewar. The fluctuations of fluid forces and fluid moment (torque) exerted on the Dewar wall of the container caused by slosh-wave excitation driven by orbital accelerations are also investigated. Since the viscous force across a liquid-solid interface and the surface-tension force across a liquid-vapor or liquid-solid interface can greatly contribute to the damping effect of slosh-wave excitation, a rotating Dewar with a baffle provides more areas of liquid-solid, and liquid-vapor, and solid-vapor interfaces than does a rotating Dewar without a baffle. Results show that the damping effect provided by the baffle reduces the amplitudes of force and moment feedback from the fluids to the container—in particular, the components of fluctuations transverse to the direction of the baffle boards.

Nomenclature

$\mathbf{a}_{gg}$	= $(a_{gg,r}, a_{gg,\theta}, a_{gg,z})$, gravity gradient vector in cylindrical coordinates
$\mathbf{a}_{gj}$	= $(a_{gj,r}, a_{gj,\theta}, a_{gj,z})$, gravity jitter vector in cylindrical coordinates
$\mathbf{d}$	= vector (not a unit vector) from the fluid element to the spacecraft mass center
(F_x, F_y, F_z)	= fluid stress force in Cartesian coordinates
f	= jitter frequency, Hz
g	= residual gravity due to jitter acceleration, as a fraction of g_0
g_B	= background gravity acceleration as a fraction of g_0
g_0	= Earth gravity acceleration, 9.81 m/s^2
h	= spacecraft orbit altitude, 650 km for GP-B
L	= height of dewar tank, cm
(L_x, L_y, L_z)	= moment arm in Cartesian coordinates
(M_x, M_y, M_z)	= fluid stress moment in Cartesian coordinates
n	= orbital rate of spacecraft, 1.07×10^{-3} rad/s for GP-B
$\mathbf{n}_\beta$	= unit vector normal to the wall
P	= thermodynamic pressure
R_c	= radius of spacecraft circular orbit, $R_E + h = 7023$ km for GP-B
R_E	= radius of the Earth, 6373 km
(r, θ, z)	= cylindrical coordinates
$\mathbf{r}_c$	= unit vector from the spacecraft mass center toward the center of the Earth
t	= time, s
$\mathbf{t}_\alpha$	= unit vector tangent to the wall
(u, v, w)	= velocity in cylindrical coordinate (cm/s)
$\delta_{\alpha\beta}$	= Kronecker delta
μ	= viscous coefficient of fluid
Π	= fluid stress
ρ	= density of fluid
τ	= spacecraft gravity turn-around time, s
τ_0	= orbital period of spacecraft, 97.6 min for GP-B
ψ_E	= azimuth angle of the Earth at the spacecraft mass center
ω	= angular velocity of spacecraft spinning about the z axis

Subscripts

L	= liquid
n	= components normal to the wall
t	= components tangent to the wall
V	= vapor
α	= direction of flowfields
β	= direction of flowfields

Superscripts

r-z	= components in the r-z plane
r-θ	= components in the r-θ plane

Received Feb. 22, 1994; revision received June 3, 1994; accepted for publication June 19, 1994.

*Professor of Mechanical and Aerospace Engineering. Associate Fellow AIAA.

†Senior Research Associate, Department of Mechanical and Aerospace Engineering.

Introduction

FOR the purpose of conducting scientific experiments, some experimental spacecraft use superconducting sensors for gyro readout and maintain instrumentation at a very low temperature (near absolute zero) for mechanical stability. The approaches to both cooling and control involve the use of superfluid liquid helium. For example, the Gravity Probe-B (GP-B) Spacecraft adopts the boiloff from the cryogenic liquid-helium Dewar as a propellant to maintain the attitude control and drag-free operation of the spacecraft.[1] Some problems with cryogenic liquid in the Dewar container can arise from asymmetry in the liquid-vapor distribution and interface fluctuations modulated by sloshing dynamics. It may be necessary to install baffle boards inside the Dewar container (as shown in Fig. 1) to reduce the degree of asymmetry in the liquid-vapor distribution.

For the case of the GP-B spacecraft, cryogenic liquid helium II, at a temperature of 1.8 K, is used as the boiloff propellant. Because of its infinite thermal conductivity, there are no temperature gradients in the liquid helium. In the absence of temperature gradients, which would drive Marangoni convection along the interface, the equilibrium shape of the free surface is governed by a balance of capillary, centrifugal, and gravitational forces. The determination of liquid-vapor interface profiles based on computational experiments can uncover details of the flow that cannot be easily visualized or measured experimentally in a microgravity environment.

Instability of the liquid surface can be induced by longitudinal and lateral accelerations, vehicle vibration, and rotational fields of the spacecraft. Thus, slosh waves are excited, producing high- and

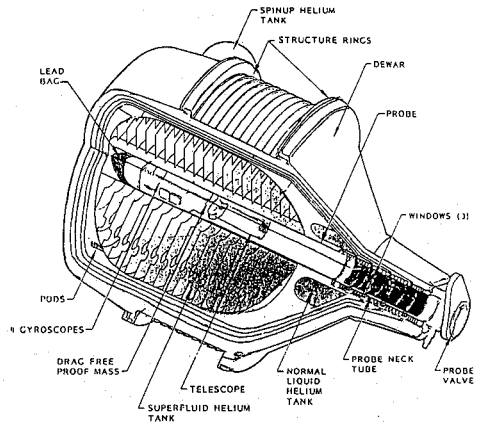

Fig. 1 GP-B module, showing the main elements of liquid-helium Dewar, probe, and baffle boards.

low-frequency oscillations in the liquid systems. The sources of the residual accelerations range from the effects of the Earth's gravity gradient, atmospheric drag on the spacecraft, and spacecraft attitude motions arising from machinery vibrations, thruster firings, crew motion, etc. A recent study[2] suggests that the high-frequency accelerations may be unimportant in comparison with low-frequency accelerations in causing residual motions.

The time-dependent dynamical behavior of rotating fluids in reduced-gravity environments was simulated by numerically solving the Navier–Stokes equations subject to the initial and boundary conditions.[3–5] At the liquid-vapor interface, both the kinematic surface boundary condition and the interface stress conditions for components tangent and normal to the interface were applied.[6–7] The initial conditions were adopted from the steady-state formulations developed by Hung et al.[3] in the geometry of the GP-B Spacecraft.[1] Some of the steady-state formulations of interface shapes were compared[8] in a free-falling aircraft (KC-135). The experiments[9] showed that the classical fluid mechanics is applicable for cryogenic liquid helium in large containers.

To study the effect of centrifugal force on the liquid helium and helium vapor for the case of the GP-B spacecraft, a spin rate of up to about 1 rpm will be imposed in the early stages of the experiment for instrument calibration. After calibration, the rotation rate will be reduced to its operational value of approximately 0.1 rpm. In the spacecraft orbit around the Earth, the azimuth angle of the Earth at the spacecraft mass center varies from 0 deg (along the axis of rotation) to 360 deg on completing an orbit; thus it requires a three-dimensional calculation.

As the spacecraft moves along the orbit, any fluid capable of motion relative to the spacecraft is subject to the acceleration that arises from the gravity gradients of the Earth.[10–12] The interaction between the particle mass of the fluid and the spacecraft mass due to gravity-gradient acceleration[11] can excite slosh waves. In this study, the characteristics of the dynamical evolution of slosh-wave excitation driven by orbital accelerations, including gravity-gradient and jitter accelerations, are investigated.

In order to reduce the degree of asymmetry in the liquid-vapor distribution and its associated disturbances due to sloshing-dynamic fluctuations driven by orbital accelerations, a number of baffle boards are installed inside the Dewar (as shown in Fig. 1). The degree of asymmetry in liquid-vapor distribution between the Dewar with and without baffle during the time period of slosh wave excitation induced by orbital accelerations acting on the spacecraft is investigated. We study the time evolution of the sloshing-dynamics-modulated viscous stress force and moment fluctuations exerted on the Dewar container in response to the orbital accelerations acting on the rotating Dewar with and without baffle.

Mathematical Model of Sloshing-Dynamics-Modulated Oscillations

Let us consider a closed circular Dewar that is partly filled with liquid helium; the ullage is helium vapor. The whole fluid system is spinning about the axis of the cylindrical coordinates. A detailed formulation of the governing equations for noninertial-frame spacecraft-bound coordinates spinning about the z axis has been given.[13–15] The dynamical forces, such as gravity-gradient, jitter, and angular accelerations and centrifugal, Coriolis, surface-tension, and viscous forces, are given explicitly there.

In the computation of the fluid forces, moment, viscous stress, and angular momentum acting on the container wall of the spacecraft, one must consider those forces and the moment in the inertial frame rather than in the noninertial frame. For the case of spin about the z axis, one must transform those vectors from the noninertial frame to the inertial frame by

$$\begin{bmatrix} F'_x \\ F'_y \\ F'_z \end{bmatrix} = \begin{bmatrix} \cos\omega t & -\sin\omega t & 0 \\ \sin\omega t & \cos\omega t & 0 \\ 0 & 0 & 1 \end{bmatrix} \begin{bmatrix} F_x \\ F_y \\ F_z \end{bmatrix} \tag{1}$$

where the prime indicates components in the inertial frame and its absence indicates components in the noninertial frame.

In order to solve sloshing-dynamic problems for liquid propellant systems in orbital spacecraft under a microgravity environment, one must solve the governing equations[13–15] accompanied by a set of initial and boundary conditions. A detailed, precise illustration of these conditions for the sloshing dynamics of fluid systems in microgravity has been given[14,16] and is not repeated in this paper. A computational algorithm applicable to cryogenic fluid management under microgravity has also been given.[6–7] To show a realistic example, a full-scale GP-B spacecraft propellant Dewar tank with an outer radius of 78 cm, an inner radius of 13.8 cm, top and bottom radii of 110 cm, and a height of 162 cm has been used in the numerical simulation. The Dewar tank is 80% filled with cryogenic liquid helium, and the ullage is helium vapor. The temperature of the helium is 1.8 K. In this study the following data were used: liquid-helium density = 0.146 g/cm^3, helium vapor density = 0.00147 g/cm^3, fluid pressure = 1.66×10^4 dyne/cm^2, surface-tension coefficient at the interface between liquid helium and helium vapor = 0.353 dyne/cm, liquid-helium viscosity coefficient = 9.61×10^{-5} cm^2/s, and contact angle = 5 deg. The initial profiles of the liquid-vapor interface for the rotating Dewar are determined from computations based on algorithms developed for the steady-state formulation of microgravity fluid management.[3–5]

A staggered grid for the velocity components is used in this computer program. The marker-and-cell method[17] of studying fluid flows along a free surface is adopted. The finite-difference method employed in this numerical study was the "hybrid scheme."[18] The formulation for this method is valid for any arbitrary interface location between the grid points and is not limited to midpoint interfaces.[19] An algorithm for a semi-implicit method[20] was used as the procedure for modeling the flowfield. The time step is determined automatically from the spacing of the grid points and the velocity of the flow fields. In order to assure the convergence of series, more than 200 iterations were applied for each time step. For the conservation of liquid volume, a deviation of less than 1% in volume was always required before a move to the next time step. A detailed description of the computational algorithm applicable to microgravity fluid management has been given.[3–5] Figures 2A and 2B show the distribution of grid points for the Dewar tank equipped with baffle boards in the radial-axial plane and the radial-circumferential plane, respectively, in cylindrical coordinates. The inner radius, outer radius, and thickness of the baffle boards chosen in this computation are 60, 78, and 1.21 cm, respectively. These five baffles are installed at locations z_1, z_2, z_3, z_4, z_5 of 43, 62, 81, 100, and 119 cm, respectively. A comparison of the mesh systems of a uniform, orthogonal grid versus a nonuniform, nonorthogonal grid indicates that there is no significant improvement in computing the velocity profile with viscous effects near the solid boundaries.

Liquid-Vapor Interface Disturbances Driven by Orbital Accelerations

Fluid systems in the orbital spacecraft are constantly affected by orbital accelerations, including gravity-gradient[10–12] and jitter[6] accelerations. In this section, both kinds of perturbations will be discussed.

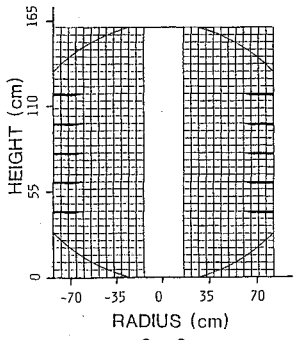

a) r-z plane at $\theta = 0$ deg

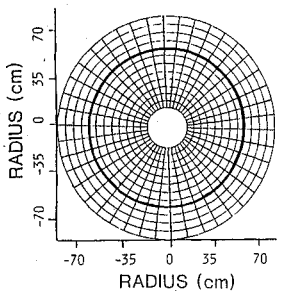

b) r-θ plane (x-y plane) at $z = L/2$

Fig. 2 Distribution of grid points in cylindrical coordinates for propellant Dewar tank equipped with baffle boards.

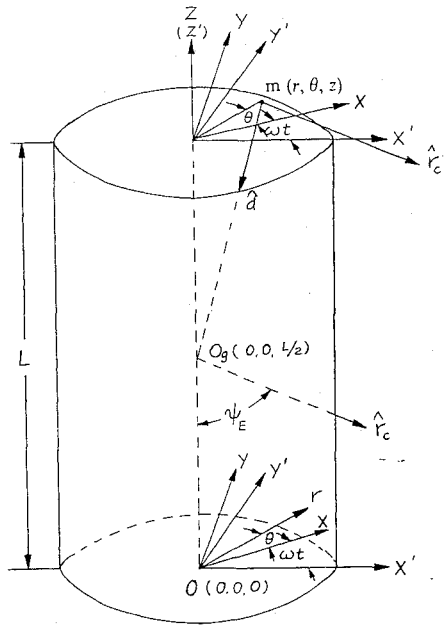

Fig. 3 Coordinate systems for the computation of gravity-gradient acceleration: (x', y', z') in inertial frame, and (x, y, z) in noninertial-frame spacecraft-bound coordinate system.

Gravity-Gradient Acceleration

For the GP-B Spacecraft, which is an Earth satellite orbiting at 650-km altitude directly over the poles, the orbital period can be computed from

$$\tau_0 = 2\pi \frac{R_c^{\frac{3}{2}}}{R_E g_0^{\frac{1}{2}}} \tag{2}$$

For the GP-B, the orbital period $\tau_0 = 97.6$ min, and the orbital rate $n = 2\pi/\tau_0 = 1.07 \times 10^{-3}$ rad/s.

The gravity-gradient acceleration acting on the fluid mass of the spacecraft can be shown to be[11]

$$\mathbf{a}_{gg} = -n^2[3(\mathbf{r}_c \cdot \mathbf{d})\mathbf{r}_c - \mathbf{d}] \tag{3}$$

For the GP-B Spacecraft, the gravity gradient exerted on the mass center of the spacecraft orbiting around the Earth on its specified orbit is assumed to be zero. In other words, the gravity acceleration exerted on the spacecraft is nothing more than the gravity-gradient acceleration defined in Eq. (3). In this study, we are interested in investigating how gravity-gradient acceleration affects the behavior of the sloshing-dynamics-governed fluid system oscillations in a rotating Dewar.

For convenience of mathematical calculation, let us describe all the parameters involved in Eq. (3) in terms of Cartesian coordinates. In order to match with the computer simulation, the mathematical derivation is considered in the first quadrant. Figure 3 illustrates the geometrical relationship of the parameters shown in Eq. (3).

The gravity-gradient acceleration at the location (r, θ, z) can be transformed[13–15] from the inertial coordinate system to the cylindrical noninertial-frame coordinates by

$$\mathbf{a}_{gg} = \begin{bmatrix} a_{gg}, r \\ a_{gg}, \theta \\ a_{gg}, z \end{bmatrix} = -n^2 \begin{bmatrix} \cos(\theta + \omega t) & \sin(\theta + \omega) & 0 \\ -\sin(\theta + \omega t) & \cos(\theta + \omega t) & 0 \\ 0 & 0 & 1 \end{bmatrix} \begin{bmatrix} 3[(z - L/2)\cos\psi_E - r\cos(\theta + \omega t)\sin\psi_E]\sin\psi_E + r\cos(\theta + \omega t) \\ r\sin(\theta + \omega t) \\ -3[(z - L/2)\cos\psi_E - r\cos(\theta + \omega t)\sin\psi_E]\cos\psi_E + (z - L/2) \end{bmatrix} \tag{4}$$

where t denotes the time.

At time $t = 0$, the rotational axis of the spacecraft is aligned with the radial direction from the Earth center to the spacecraft mass center. For the GP-B, the spin axis of the Dewar is constantly sighted on Rigel, a bright star in Orion. Thus, the azimuth angle ψ_E is in coincidence with the orbiting motion of the spacecraft and can be expressed as

$$\psi_E = \frac{R_E g_0^{\frac{1}{2}}}{R_c^{\frac{3}{2}}} t = nt \qquad \text{(rad)} \tag{5}$$

where the time t is measured from the instant when the spacecraft spin axis is aligned with the radial direction from the spacecraft mass center to the center of the Earth. In other words, for the case of the GP-B, the azimuth angle is the angle between the spin axis of the spacecraft and the radial vector from the spacecraft mass center to the center of the Earth.

It is interesting to note the characteristics of gravity-gradient acceleration. According to Eq. (4), the gravity-gradient acceleration[11] acting on any element of fluid mass inside the container increases two units per unit of distance measured from the mass center of the container (point O_g in Fig. 3) to the location of the mass element, parallel to the vector from the Dewar mass center to the center of the Earth (parallel to the unit vector $\mathbf{r}_c$ shown in Fig. 3). Meanwhile, the acceleration acting on the fluid mass decreases one unit per unit of the shortest distance measured from the location of the fluid mass to the axis along the vector from the Dewar mass center to the center of the Earth.[11] For example, the orbital period of the GP-B spacecraft is 97.6 min (= 5856 s), and the numerical simulation of this paper is planned to be carried out for a quarter of the period, which is 1464 s. Figures 4Aa–4Ac show the time variation of the gravity-gradient acceleration in the x, y and z components, respectively, in an example of a time period of a quarter orbital period along the GP-B orbit with 0.1-rpm Dewar spin speed, acting on the fluid mass located at $(r, \theta, z) = (20\text{ cm}, \pi/4, 10\text{ cm})$. In this figure, the solid line indicates the time evolution of full gravity-gradient acceleration, the dotted line the gravity-gradient acceleration with $\omega = 0$, and the broken line the gravity-gradient acceleration with $\psi_E = 0$. When $\omega = 0$, the gravity-gradient acceleration behaves as a driver of the tidal motion. For $\omega \neq 0$, the gravity-gradient acceleration provides a constant torsional moment (different values for the fluid element at different locations) acting

on the fluid element with the spin axis constantly pointing toward the center of the Earth for a fluid element fixed in the moving coordinates. Sinusoidal oscillations shown for the x, y, and z components of full gravity-gradient acceleration (solid line) in the figure with peaks located at about 300, 600, 900, and 1200 s are characterized by the angular velocity of 0.1-rpm spin rate of the Dewar container imposed on the fluid element. Also, the magnitude increment of the z component (along the spin axis) of the gravity-gradient acceleration, increasing as a quarter of a sinusoidal wave, simulates a quarter orbital period of the spacecraft orbital motion during 1500 s of time-dependent fluctuations. The magnitude and the direction of the gravity-gradient acceleration acting on each fluid mass element are strongly dependent upon how far the location of the element deviates from the Dewar mass center along the axis parallel to the vector $\mathbf{r}_c$, which varies with time. Thus the gravity-gradient acceleration acting on the fluid is anticipated to be different at different locations in the container. Figure 4a also shows that the magnitude of the gravity-gradient acceleration is on the order of $10^{-7}\ g_0$ for the GP-B spacecraft. It is noted that the centrifugal force generated by the spinning of the container is $r\omega^2$, which is $8.7 \times 10^{-6}\ g_0$ with $\omega = 0.1$ rpm and $r = 78$ cm for the outer radius of the Dewar container. In other words, the centrifugal force is 87 times greater than the gravity-gradient force for the case of the GP-B spacecraft.

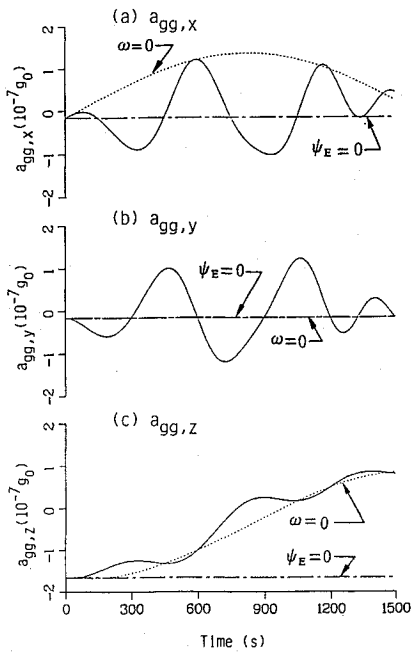

a) Gravity gradient acceleration

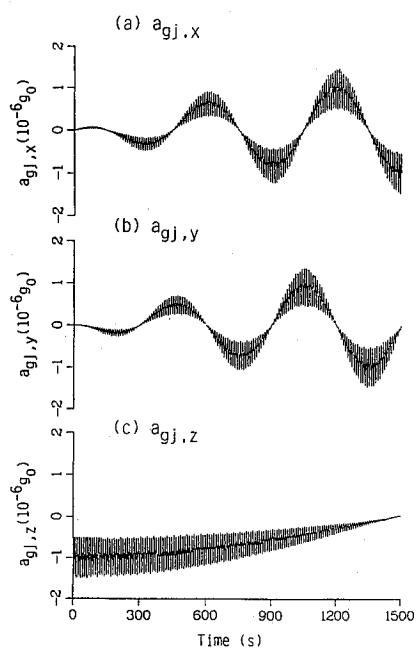

b) Gravity jitter acceleration

Fig. 4 a) Time variation of gravity-gradient acceleration acting on a fluid mass element located at $(r, \theta, z) = (20\text{ cm}, \pi/4, 10\text{ cm})$ for a quarter of an orbital period and b) time variation of jitter acceleration acting on the fluid system with an amplitude of $10^{-6}\ g_0$.

Jitter Accelerations

In addition to gravity-gradient acceleration,[10–12] there are jitter accelerations, which include atmospheric drag on the spacecraft, solar-wind interaction with the spacecraft atmospheric environment during minima and maxima in the solar cycle, and spacecraft guidance and attitude motions arising from machinery vibrations, thruster firings, crew motions, etc. These perturbations act on the on-orbit fluid systems. Fluctuations of residual gravity due to jitter acceleration are modeled by

$$g = g_B\left[1 + \tfrac{1}{2}\sin(2\pi f t)\right] \tag{6}$$

In this study, jitter acceleration with equivalent gravity acceleration of $10^{-6}\ g_0$ due to various intensities of spacecraft atmospheric drag and other forces has been considered. A rotation speed of 0.1 rpm for normal GP-B spacecraft operation is chosen as an example. Three frequencies of gravity jitter with the values[10] 0.1, 1.0, and 10 Hz have also been considered for the investigation of bubble oscillations modulated by sloshing dynamics. The components of gravity-jitter acceleration with modification of the azimuth angle and rotation in the noninertial coordinate system are given by

$$\begin{aligned}\mathbf{a}_{gj} &= (a_{gj,r}, a_{gj,\theta}, a_{gj,z}) \\ &= [g\sin\psi_E\cos(\theta+\omega t), -g\sin\psi_E\sin(\theta+\omega t), -g\cos\psi_E]\end{aligned} \tag{7}$$

The characteristics of gravity-gradient and jitter accelerations, shown in Eqs. (4) and (7), respectively, are quite different. While gravity-gradient acceleration imposes different values of acceleration on the fluid mass at different locations in the container, gravity-jitter acceleration imposes the same acceleration everywhere. Figure 5 shows the time variation of gravity-jitter acceleration with

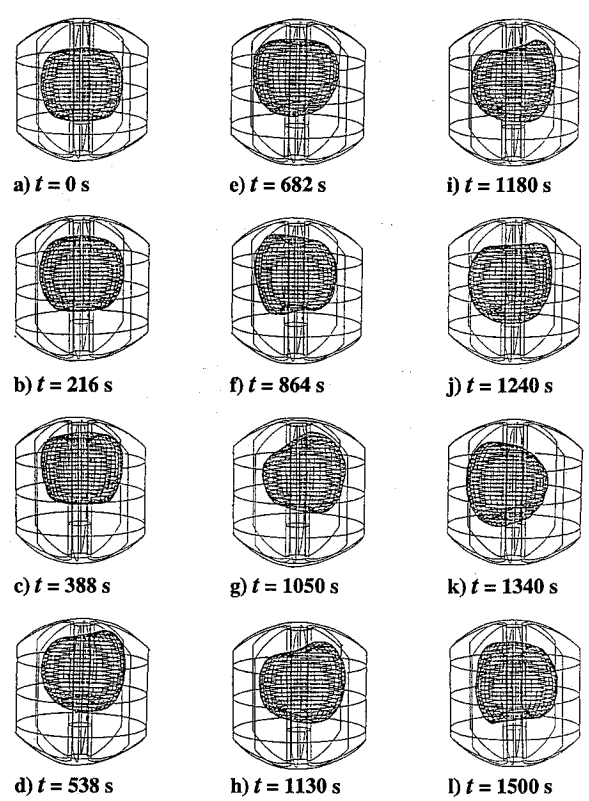

Fig. 5 Time evolution of the three-dimensional liquid-vapor interface oscillations driven by gravity jitter ($g = 10^{-6}\ g_0$) and gravity gradient, without baffles.

a magnitude of 10^{-6} g_0 for an orbit period of 5856 s with a container rotation speed of 0.1 rpm and a jitter frequency of 0.1 Hz for components along x, y, and z directions acting on the fluid mass everywhere in the container. During a quarter-orbit period of sloshing-dynamic simulation, it can be seen from Fig. 4B that the jitter accelerations are basically sinusoidal along the x and y directions. There is a strong downward acceleration applied to z axis at the very beginning, which gradually decreases to zero and becomes an upward acceleration at the end of the first quarter and the beginning of the second quarter of the orbital period.

Interface Oscillations Without Installing Baffle Boards

In this study, the time evolution of the liquid-vapor interface oscillations due to sloshing dynamics has been investigated. These dynamics are driven by orbital accelerations of combined gravity-gradient and jitter accelerations with magnitude 10^{-6} g_0 and 0.1-Hz jitter frequency associated with the spinning motion. The initial configuration of the liquid-vapor interface with and without installing baffle boards is based on a computation with the numerical algorithm developed in our earlier studies.[3–5] The time period of numerical computation covered in this study constitutes a quarter of the total orbital period of the spacecraft.

Figure 5 shows the time evolution of the three-dimensional dynamical behavior of the liquid-vapor interface oscillations driven by orbital gravity-gradient and jitter accelerations acting on a rotating Dewar without a baffle. For convenience of comparison, liquid-vapor interface profiles with the same values of the time sequences as in earlier investigations are presented. The time sequences chosen throughout this paper are at t = 0, 216, 388, 538, 682, 864, 1050, 1130, 1180, 1240, 1340, and 1500 s during a quarter of the spacecraft orbital period. The figure clearly shows that there is a series of asymmetric oscillations excited along the surface of the liquid-vapor interface by orbital accelerations.

We have made careful a examination of Fig. 5 for the case of bubble oscillations dominated by gravity-jitter acceleration, in comparison with the major driving force of gravity jitter acceleration, during a quarter of the spacecraft orbital period, shown in Fig. 4b. The results indicate that there is a sinusoidal oscillation longitudinal to the direction along the line joining the spacecraft mass center with the Earth's center (parallel to the unit vector $\mathbf{r}_c$ shown in Fig. 3). As shown in Eq. (5), the angle ψ_E varies with time. The components of jitter acceleration decomposed into (x, y, z) coordinates show that there are sinusoidal oscillations along the x and y directions while a strong negative component of acceleration is applied to the z axis during a quarter of the spacecraft orbital period (see Fig. 5). This phenomenon shows that the jitter acceleration exerted on the spacecraft is equivalent to time-dependent oscillatory forces. These forces push the bubble in the leftward and rightward movement of oscillations along the x and y axes while there is a upward motion of the bubble along the z axis during a quarter orbital period of the spacecraft.

In addition to the 0.1-Hz (low-frequency) gravity-jitter-dominated acceleration, liquid-vapor interface oscillations driven by 1.0-Hz (medium-frequency) and 10-Hz (high-frequency) gravity-jitter-dominated acceleration have also been investigated. The characteristics of these three ranges of gravity-jitter frequencies have been well documented in the earlier studies.[3,4] Thus these oscillations will not be treated in this paper. The results show that the lower-frequency gravity-jitter-dominated acceleration contributes more to the driving of asymmetrical profiles of the interface than does the higher-frequency acceleration. These results are in agreement with the earlier studies.[3,4]

Interface Oscillations for a Dewar with a Baffle

For the purpose of reducing the degree of asymmetry in the liquid-vapor distribution, a series of baffle boards are installed in the Dewar with dimensions shown in Fig. 2. The remaining conditions are similar to the Dewar without a baffle, as discussed earlier.

Figure 6 shows the time evolution of the three-dimensional dynamical behavior of the liquid-vapor interface oscillations. These oscillations are driven by orbital acceleration, including gravity-gradient and jitter accelerations, with an amplitude of 10^{-6} g_0 and a jitter frequency of 0.1 Hz, for 0.1-rpm spin of a rotating Dewar equipped with a baffle board. A comparison of the results presented in Figs. 5 and 6 shows that a greater degree of asymmetry is obtained for the sloshing dynamics governing liquid-vapor interface fluctuations in a rotating Dewar without a baffle.

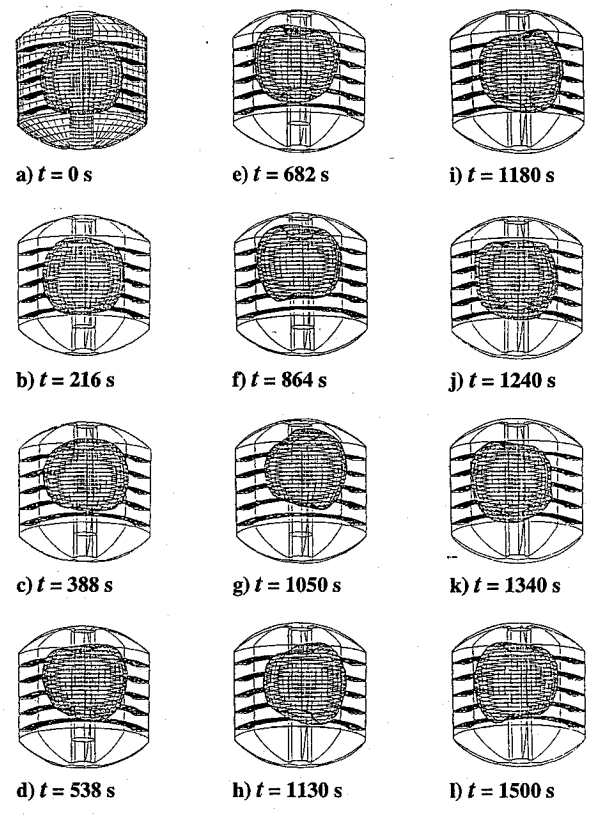

Fig. 6 Time evolution of three-dimensional liquid-vapor interface oscillations driven by gravity jitter ($g = 10^{-6}$ g_0) and gravity gradient, with baffles.

A comparison of sloshing-dynamics-modulated bubble fluctuations driven by orbital accelerations, including gravity-gradient and jitter accelerations, for a Dewar without and with baffle leads to the following conclusions:

1) A sinusoidal torsional moment activated by orbital accelerations dominated by jitter acceleration with spinning motion exerted on the rotating Dewar container produces greater values of sloshing fluctuations in the absence of a baffle.

2) Vertical movement of eccentric-wheel bubble oscillations in a rotating Dewar results from the sloshing-dynamics-modulated bubble disturbances actuated by orbital accelerations dominated by jitter accelerations.

In this study, the bubble is small enough to rotate freely in the Dewar without intersecting the baffle boards. As the liquid fill level becomes lower, the size of the bubble will be great enough to intersect with the baffle boards. These cases have been illustrated in our recent studies.[7,21] These studies show that the present investigation is equally applicable to large and to small bubbles.

Mathematical Formulation of Fluid Forces and Moment Fluctuations Due to Slosh Waves

For the purpose of considering large-amplitude slosh-wave-activated fluid force fluctuations exerted on the solid walls of the Dewar, the fluid forces are decomposed into the wall tangential and normal components as

$$\Pi_t = \mu\left(\frac{\partial u_\alpha}{\partial x_\beta} + \frac{\partial u_\beta}{\partial x_\alpha}\right)\mathbf{t}_\alpha \cdot \mathbf{n}_\beta \tag{8}$$

$$\Pi_n = \left[P\delta_{\alpha\beta} - \mu\left(\frac{\partial u_\alpha}{\partial x_\beta} + \frac{\partial u_\beta}{\partial x_\alpha}\right)\right]\mathbf{n}_\alpha \cdot \mathbf{n}_\beta \tag{9}$$

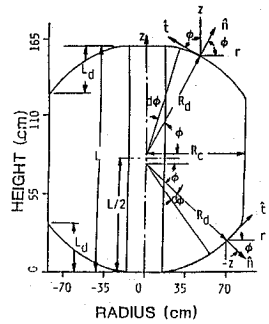

a) r-z plane at $\theta = 0$ deg

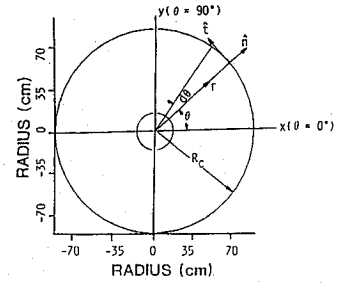

b) r-θ plane (x-y plane) at $z = L/2$

Fig. 7 Geometry of Gravity Probe-B Spacecraft propellant Dewar container with coordinate system perpendicular and tangent to the container wall.

Figures 7a and 7b show the geometry of the GP-B Dewar propellant tank as an example in the r-z and r-θ planes, respectively. In order to make the computation of fluid forces match the geometry of the Dewar tank, the mathematical formulation has been divided into three sections: 1) the top wall (dome) section, 2) the bottom wall (dome) section, and 3) the cylindrical section (including the probe section of the inner wall of the Dewar).

1) Top wall (dome) section:

$$(\Pi_t)^{r\text{-}z}_{\text{top wall}} = \mu\left(\frac{\partial u}{\partial z} + \frac{\partial w}{\partial r}\right)\cos 2\phi \tag{10}$$

$$(\Pi_t)^{r\text{-}\theta}_{\text{top wall}} = \mu\left[\left(\frac{1}{r}\frac{\partial u}{\partial \theta} + \frac{\partial v}{\partial r}\right)\cos\phi + \left(\frac{1}{r}\frac{\partial w}{\partial \theta} + \frac{\partial v}{\partial z}\right)\sin\phi\right] \tag{11}$$

$$(\Pi_n)_{\text{top wall}} = P + \mu\left(\frac{\partial u}{\partial z} + \frac{\partial w}{\partial r}\right)\sin 2\phi \tag{12}$$

2) Bottom wall (dome) section:

$$(\Pi_t)^{r\text{-}z}_{\text{bottom wall}} = \mu\left(\frac{\partial u}{\partial z} + \frac{\partial w}{\partial r}\right)\cos 2\phi \tag{13}$$

$$(\Pi_t)^{r\text{-}\theta}_{\text{bottom wall}} = \mu\left[\left(\frac{1}{r}\frac{\partial u}{\partial \theta} + \frac{\partial v}{\partial r}\right)\cos\phi - \left(\frac{1}{r}\frac{\partial w}{\partial \theta} + \frac{\partial v}{\partial z}\right)\sin\phi\right] \tag{14}$$

$$(\Pi_n)_{\text{bottom wall}} = P - \mu\left(\frac{\partial u}{\partial z} + \frac{\partial w}{\partial r}\right)\sin 2\phi \tag{15}$$

3) Cylindrical section (including probe section of inner wall of the Dewar):

$$(\Pi_t)^{r\text{-}z}_{\text{cylindrical}} = \mu\left(\frac{\partial u}{\partial z} + \frac{\partial w}{\partial r}\right) \tag{16}$$

$$(\Pi_t)^{r\text{-}\theta}_{\text{cylindrical}} = \mu\left(\frac{1}{r}\frac{\partial u}{\partial \theta} + \frac{\partial v}{\partial r}\right) \tag{17}$$

$$(\Pi_n)_{\text{cylindrical}} = P \tag{18}$$

The velocity components in cylindrical coordinates (r', θ', z') are shown as (u', v', w') in the inertial frame rather than in the noninertial frame for the purpose of computing fluid forces acting on the container. Note that all the velocity components are expressed in the inertial frame only.

To accommodate the spacecraft dynamics of pitch (x), yaw (y) and roll (z), cylindrical coordinates (shown in Fig. 7) of the rotating container are transformed into Cartesian coordinates based on $(x, y, z) = (r\cos\theta, r\sin\theta, z)$ with corresponding velocity components $(v_x, v_y, v_z) = (u\cos\theta - v\sin\theta, u\sin\theta + v\cos\theta, w)$. For the GP-B Spacecraft, the axis of rotation is always fixed at the point of the proof mass, which is located at the geometrical center of the Dewar at $(x_c, y_c, z_c) = (0, 0, L/2)$, where L is the height of the Dewar (see Fig. 7). To fulfill this goal, the stress distributions, shown in Eqs. (8) to (18), have to be decomposed in the x, y, z directions and yield the force (F_x, F_y, F_z). A detailed mathematical derivation of (F_x, F_y, F_z) is shown in our recent publication[7] and will not be repeated.

The moment of fluid force acting on the wall of the Dewar container can be computed from the cross product of the moment arm (the perpendicular distance from the location of the proof mass to the total force) and the total force. Again a detailed mathematical derivation of the moment of the fluid force (M_x, M_y, M_z) acting on the Dewar wall of the spacecraft has been given[7] and will not be repeated herein.

The components of the moment can be written as the following expression:

$$\begin{bmatrix} M_x \\ M_y \\ M_z \end{bmatrix} = \begin{bmatrix} L_y F_z - \left(L_z - \frac{L}{2}\right)F_y \\ \left(L_z - \frac{L}{2}\right)F_x - L_x F_z \\ L_x F_y - L_y F_x \end{bmatrix} \tag{19}$$

where L_x, L_y, and L_z denote the components of the moment arm along the x, y, and z axes, respectively.

Characteristics of the Slosh-Wave-Associated Fluid Force and its Moment Fluctuations Exerted on the Dewar Container

From the previous discussions, one can calculate the fluid forces and the associated moments exerted on the Dewar container of the spacecraft propellant tank. Figures 8a(a)–8a(c) show the computed time variation of the fluctuations of the fluid forces along the x, y, and z axes, respectively. The fluctuations are exerted on the Dewar container and result from accelerations dominated by jitter acceleration acting on the rotating Dewar without a baffle during the course of a quarter orbital period. The figure shows the following results:

1) the fluid force fluctuations are $(\Delta F_x, \Delta F_y, \Delta F_z) = (1134, 1211, 891)$ dynes, so that $\Delta F_y > \Delta F_x > \Delta F_z$. The maximum absolute values of fluid forces are $\max(|F_x|, |F_y|, |F_z|) = (635, 642, 746)$ dynes, so that $|F_z| > |F_y| > |F_x|$.

2) The initial values of F_x and F_y start at zero, while those of F_z start at a nonzero value. This result is due to the fact that the shape of the rotating bubble is asymmetric with respect to the x and y axes, which makes F_x and F_y equal to zero at time $t = 0$ while the resultant force along the rotating axis of z is not equal to zero because of preexisting orbital accelerations along the z axis at $t = 0$.

3) The characteristics of the induced fluid force that is exerted on the cntainer wall along the x, y, and z axes follow the trends of jitter-dominated accelerations. These accelerations are shown in Fig. 4B and are amplified and damped by the sloshing-dynamic modulations through the bubble oscillations. This information is particularly important when the spacecraft propellant system is partly filled with liquid propellant.

4) A comparison of Figs. 4b and 8a shows that Fig. 4b represents the input jitter-dominated acceleration forces, and Fig. 8a the resulting input force exerted on the Dewar container through the sloshing-dynamic modulator consisting liquid helium not filling the container. The coupling between surface tension and viscosity in the sloshing-dynamic modulation of fluid systems is very similar

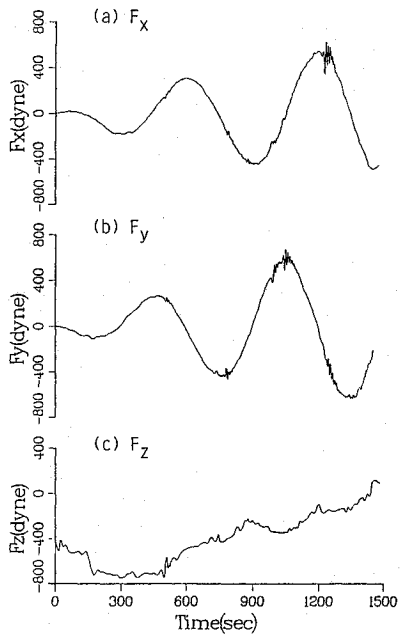

a) Without baffle

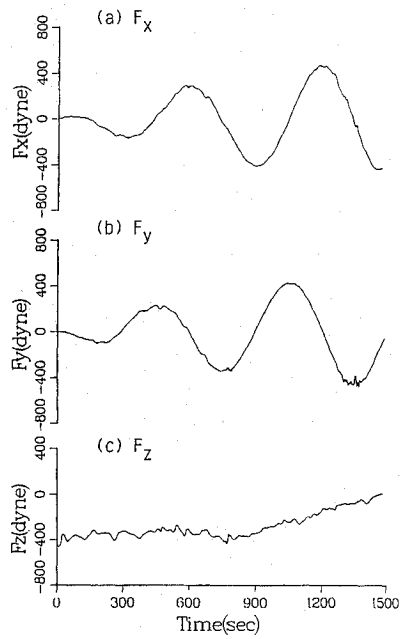

b) With baffle

Fig. 8 Time sequence of the fluctuations of fluid stress forces exerted on the Dewar container.

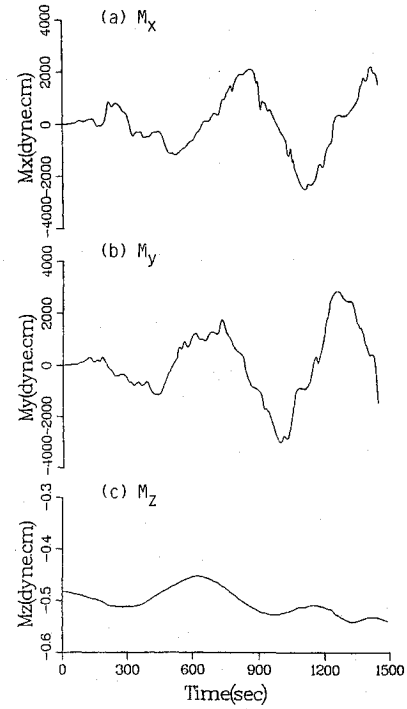

a) Without baffle

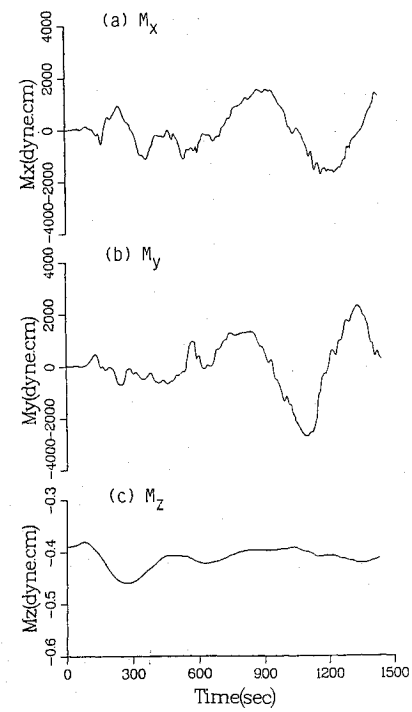

b) With baffle

Fig. 9 Time sequence of the fluctuation of fluid stress moments exerted on the Dewar container.

to the coupling of a mass spring and damper in the solid dynamics of oscillating systems. Figure 8A shows how the input force fluctuations have been modulated by the amplification and damping processes through the surface-tension and viscosity effects in the Dewar partly filled with liquid helium.

The computed time variations of the fluctuations of fluid force moments that are exerted on the Dewar container along the x, y, and z axes are shown in Figs. 9a(a)–9a(c), respectively. The moments are induced by orbital accelerations dominated by jitter acceleration acting on the rotating Dewar without a baffle. The values of the fluid force moment fluctuations exerted on the Dewar are $(\Delta M_x, \Delta M_y, \Delta M_z) = (5.24, 5.97, 10^{-4}) \times 10^3$ dyne-cm. The maximum absolute values of the fluid force moment exerted on the Dewar are $\max(|M_x|, |M_y|, |M_z|) = (2.94, 3.04, 5 \times 10^{-4}) \times 10^3$ dyne-cm. These comparisons show $\Delta M_y > \Delta M_x \gg \Delta M_z$ and $|M_y| > |M_x| \gg |M_z|$. As M_y, M_x, and M_z are determined by the components (F_x, L_z, F_z, L_x), (F_z, L_y, F_y, L_z), and (F_y, L_x, F_x, L_y), respectively, the time averages of L_x and L_y were shown to approach zero. This explains why the moment $M_z = L_x F_y - L_y F_x \approx 0$ even though there is a rolling moment with angular velocity 0.1 rpm due to which the induced rolling moment exerted by the viscous rotating fluid is small in comparison with the induced pitch and yaw moments due to the sloshing dynamics of modulated bubble oscillations.

Figures 8 and 9 show the total forces and torques exerted on the Dewar container from the fluid side in response to the orbital acceleration through the modulation by sloshing dynamics.

Fluctuations of the fluid force and torque exerted on the rotating Dewar with baffle boards and driven by the orbital accelerations dominated by jitter acceleration acting on the Dewar have also been investigated. Figures 8b(a)–8b(c) show the computed

time variations of these fluctuations. The values of the fluid forces are $(\Delta F_x, \Delta F_y, \Delta F_z) = (895, 908, 445)$ dynes, and $\max(|F_x|, |F_y|, |F_z|) = (483, 486, 459)$ dynes. These comparisons show $\Delta F_y > \Delta F_x > \Delta F_z$ and $|F_y| > |F_x| > |F_z|$. The results concluded from Fig. 8b are similar to those concluded from Fig. 8a except that the damping effects modulated by the baffle boards, with regard to the magnitudes and fluctuations of forces transverse and longitudinal to the rotating axis, are quite different. A comparison of Figs. 8a and 8b for both fluid forces and fluid-force fluctuations exerted on the Dewar between rotating Dewar with and without baffle leads to the following conclusions: 1) the baffle boards decrease the fluctuations of force components transverse to the rotating axis by 25%; 2) the baffle boards decrease the fluctuations of components longitudinal to the rotating axis by as much as 45%. These results are due to the fact that the baffle boards are placed transverse to the rotation axis. They imply that the baffle boards can be used as an effective damper and also that the damping effect is strongly dependent upon the shape and the geometrical arrangement of the baffles.

Figures 9b(a)–9b(c) show the computed time variations of the fluid-force moment exerted on the Dewar container along the x, y, and z axes, respectively. These variations are induced by orbital accelerations dominated by acceleration acting on a rotating Dewar with a baffle. The values of the fluid-force moment fluctuations and the maximum absolute values of fluid moments are $(\Delta M_x, \Delta M_y, \Delta M_z) = (2.94, 4.47, 8 \times 10^{-5}) \times 10^3$ dyne-cm, and $\max(|M_x|, |M_y|, |M_z|) = (1.61, 2.44, 4 \times 10^{-4}) \times 10^3$ dyne-cm. Comparison shows that $\Delta M_y > \Delta M_x > \Delta M_z$ and $|M_y| > |M_x| > |M_z|$. The results concluded from Fig. 9b are similar to those concluded from Fig. 9a. A comparison of Figs. 9a and 9b for both fluid moments and moment fluctuations exerted on the Dewar container, between a rotating Dewar with and without baffle, shows that the characteristics of these two curves are also very similar. However, the components of fluid-moment fluctuations transverse to the rotating axis for the Dewar with a baffle are less than 70% of the values of fluctuations without a baffle. There is no fluid moment exerted on the Dewar with a component longitudinal to the axis. This result also implies that the baffle boards can be used as an effective damper in this case.

Discussion and Conclusion

The dynamical behavior of a sloshing-dynamics-governed cryogenic liquid system driven by the orbital accelerations dominated by jitter acceleration has been studied. An example applicable to time-dependent variations in the GP-B Spacecraft Dewar with and without baffle has been computed with the three-dimensional Navier–Stokes equations subject to initial and boundary conditions. The initial condition for the liquid-vapor interface profiles were adopted from the steady-state formulation of an existing investigation.[6,7]

In this study, a computation is conducted throughout a quarter orbit period for an orbiting spacecraft. Results of slosh-wave excitation along the liquid-vapor interface induced by orbital accelerations dominated by jitter acceleration indicate the following: 1) the jitter acceleration exerted on the spacecraft is a time-dependent torsional moment with leftward and rightward movement of oscillations along the x and y axes, and 2) there is an upward motion of the bubble along z axis during the period of a quarter orbit of the spacecraft.

The fluid force and fluid moment that are exerted on the Dewar wall with and without baffle lead to the following results: 1) there are components of forces and torques along the yaw and pitch axes excited by slosh-wave excitation driven by jitter acceleration in a partly liquid-filled container, and 2) there is also a component of forces and torques contributing to the existing rotation about the roll axis. Results show that there is a series of large-amplitude fluctuations of fluid forces and fluid moments exerted on the Dewar container of a spacecraft propellant tank, which in turn disturbs the dynamics of the spacecraft along the yawing and pitching axes. In particular, slosh waves induced by jitter acceleration contribute greatly to the excitation of large-amplitude fluctuations of fluid forces and fluid moments exerted on the container and to the perturbations of spacecraft dynamics along the pitch and yaw axes, as well as to the existing rotation about the rolling axis of the spacecraft.

Since a viscous force (across the liquid-solid interface) and surface-tension force (across the liquid-vapor and liquid-solid interfaces) can greatly contribute to the damping effect of slosh-wave excitation, a rotating Dewar with a baffle provides more area of liquid-solid, liquid-vapor, and solid-vapor interfaces than does a Dewar without a baffle. The present results show that a baffle significantly reduces the fluctuations of both fluid force and fluid moment (torque) with components transverse to the direction of the baffle boards.

The time-dependent variations of orbital accelerations imposed on the spacecraft will change the asymmetry of the distribution of the liquid and vapor in the rotating Dewar container. This means that both the fluid forces and the fluid moments exerted on the spacecraft will be greatly disturbed by the presence of asymmetric fluctuations in the liquid-vapor interface. In this study, it has been shown that a rotating Dewar equipped with a baffle can provide a greater damping to inhibit the development of large-amplitude slosh waves along the liquid-vapor interface.[21,22] Proper installation of baffle boards in the rotating Dewar has shown that the fluid-force and fluid-moment fluctuations can be significantly reduced. This is particularly, true for the components of fluctuations transverse to the direction of the baffle boards. An investigation of the effects of the number, geometry, and size of baffles, and also their spacing, on the damping of sloshing will be reported in subsequent papers.

Acknowledgments

The authors appreciate the support received from NASA Grant NAG8-938 and Contract NAS8-38609/Delivery Order No. 103. They would like to express their gratitude to Richard A. Potter of NASA Marshall Space Flight Center for stimulating discussions during the course of the present study.

References

[1]Wilkinson, D. T., et al., "Gravitation, Cosmology and Cosmic-Ray Physics," *Physics Today*, Vol. 39, No. 1, 1986, pp. 43–46.

[2]Kamotani, Y., Prasad, A., and Ostrach, S., "Thermal Convection in an Enclosure Due to Vibrations aboard a Spacecraft," *AIAA Journal*, Vol. 19, No. 4, 1981, pp. 511–516.

[3]Hung, R. J., Lee, C. C., and Leslie, F. W., "Response of Gravity Level Fluctuations on the Gravity Probe-B Spacecraft Propellant System," *Journal of Propulsion and Power*, Vol. 7, No. 4, 1981, pp. 556–564.

[4]Hung, R. J., and Shyu, K. L., "Space-Based Cryogenic Liquid Hydrogen Reorientation Activated by Low Frequency Impulsive Reverse Thruster of Geyser Initiation," *Acta Astronautica*, Vol. 25, No. 5, 1991, pp. 709–719.

[5]Hung, R. J., and Shyu, K. L., "Constant Reverse Thrust Activated Reorientation of Liquid Hydrogen with Geyser Initiation," *Journal of Spacecraft and Rockets*, Vol. 29, No. 2, 1992, pp. 279–285.

[6]Hung, R. J., Lee, C. C., and Leslie, F. W., "Similarity Rules in Gravity Jitter-Related Spacecraft Liquid Propellant Slosh Wave Excitation," *Journal of Fluids and Structures*, Vol. 6, No. 3, 1992, pp. 493–522.

[7]Hung, R. J., Lee, C. C., and Leslie, F. W., "Effect of the Baffle on the Spacecraft Fluid Propellant Viscous Stress and Moment Fluctuations," *Transactions of the Japan Society for Aeronautical and Space Sciences*, Vol. 35, No. 1, 1993, pp. 187–207.

[8]Leslie, F. W., "Measurements of Rotating Bubble Shapes in a Low Gravity Environment," *Journal of Fluid Mechanics*, Vol. 161, No. 2, 1985, pp. 269–279.

[9]Mason, P., Collins, D., Petrac, D., Yang, L., Edeskuty, F., Schuch, A., and Williamson, K., "The Behavior of Superfluid Helium in Zero Gravity," *Proceedings of the 7th International Cryogenic Engineering Conferences*, Science and Technology Press, Surrey, England, UK, 1978.

[10]Avduyevsky, V. S. (ed.), *Scientific Foundations of Space Manufacturing*, MIR, Moscow, 1984.

[11]Forward, R. L., "Flattening Space-Time Near the Earth," *Physical Review A*, Vol. 26, No. 5, 1982, pp. 735–744.

[12]Misner, C. W., Thorne, K. S., and Wheeler, J. A., *Gravitation*, Freeman, San Francisco, 1973, pp. 1–1279.

[13]Hung, R. J., and Pan, H. L., "Differences in Gravity-Gradient and Gravity Jitter-Excited Slosh Waves in Microgravity," *Transactions of the Japan Society for Aeronautical and Space Sciences*, Vol. 36, No. 1, 1993, pp. 153–169.

[14]Hung, R. J., Pan, H. L., and Leslie, F. W., "Gravity-Gradient or Gravity Jitter Induced Viscous Stress and Moment Fluctuations in Microgravity," *Fluid Dynamics Research*, Vol. 14, No. 1, 1994, pp. 29–51.

[15]Hung, R. J., and Lee, C. C., "Effect of Baffle on Gravity-Gradient Acceleration Excited Slosh Waves in Microgravity," *Journal of Spacecraft and Rockets*, Vol. 31, No. 6, 1994, pp. 1107–1114.

[16]Hung, R. J., and Pan, H. L., Asymmetric Slosh Wave Excitation in Liquid-Vapor Interface under Microgravity, *Acta Mechanica Sinica*, Vol. 9, No. 2, 1993, pp. 298–311.

[17]Harlow, F. H., and Welch, F. E., "Numerical Calculation of Time-Dependent Viscous Incompressible Flow of Fluid with Free Surface," *Physics of Fluids*, Vol. 8, No. 11, 1965, pp. 2182–2189.

[18]Spalding, D. B., "A Novel Finite-Difference Formulation for Differential Expressions Involving Both First and Second Derivatives," *International Journal of Numerical Methods in Engineering*, Vol. 4, No. 3, 1972, pp. 551–559.

[19]Patanker, S. V., *Numerical Heat Transfer and Fluid Flow*, McGraw-Hill, New York, 1980, p. 197.

[20]Patanker, S. V., and Spalding, S. D., "A Calculation Procedure for Heat, Mass and Momentum Transfer in Three Dimensional Parabolic Flows," *International Journal of Heat and Mass Transfer*, Vol. 15, No. 6, 1972, pp. 1787–1805.

[21]Hung, R. J., Lee, C. C., and Leslie, F. W., "Effect of the Baffle on the Asymmetric Gravity-Jitter Excited Slosh Waves and Spacecraft Moment and Angular Momentum Fluctuations," *Journal of Aerospace Engineering*, Vol. 207, No. 1, 1993, pp. 105–120.

[22]Hung, R. J., Lee, C. C., and Leslie, F. W., "Spacecraft Dynamical Distribution of Fluid Stresses Activated by Gravity Jitters Induced Slosh Waves," *Journal of Guidance, Control, and Dynamics*, Vol. 15, No. 4, 1992, pp. 817–824.

[23]Hung, R. J., and Pan, H. L., "Fluid Force Activated Spacecraft Dynamics Driven by Gravity-Gradient and Jitter Accelerations in Microgravity," *Journal of Guidance, Control, and Dynamics* (to be published).

T. C. Lin
Associate Editor